Supplementary Material

THEORY

1 Helical shape and fluctuations of a free FtsZ filament

To represent the structure of a long filaments, we use the parametric form of the helix

$$\mathbf{r}(\phi) = (R\ cos\phi, R\ sin\phi, \lambda\phi)\,, \tag{S1}$$

with the helical axis along the Z direction and the angle ϕ measured around that axis. The parameters R and λ give the cylindrical radius and the screw thread of the helix, respectively. The tangent unit vector at any point of the helix is

$$\mathbf{T} = \frac{1}{\sqrt{R^2+\lambda^2}}\,(-R\ sin\phi, R\ cos\phi, \lambda)\,, \tag{S2}$$

and the filament length for any variation ϕ of the axial angle is $s = \sqrt{R^2+\lambda^2}\ \phi$.

The constant main curvature ρ of the helix is obtained from the derivative of $\mathbf{T}$ with respect to length s,

$$\rho = \left|\frac{d\mathbf{T}}{ds}\right| = \frac{R}{R^2+\lambda^2}. \tag{S3}$$

The torsion τ is given by the change in the tangent plane,

$$\tau = \frac{1}{\rho}\left|\mathbf{T}\times\frac{d\mathbf{T}}{ds}\right| = \frac{\lambda}{R^2+\lambda^2}. \tag{S4}$$

The parameters of the helix in (S1), $R = \rho/(\rho^2+\tau^2)$ and $\lambda = \tau/(\rho^2+\tau^2)$, may be extracted from the mean values $\langle\theta\rangle$ and $\langle\delta\rangle$. The angle θ corresponds to the change in the direction of $\mathbf{T}(s)$ over the distance covered by a FtsZ monomer, $s = d \approx 4.5nm$, so that

$$\rho \approx \left|\frac{\mathbf{T}(d)-\mathbf{T}(0)}{d}\right| = \frac{\langle\theta\rangle}{d} \approx 0.029nm^{-1}. \tag{S5}$$

If the tangential plane were fixed, the filament would form a ring with radius $1/\rho \approx 34nm$, i.e. of about 40 or 50 monomers length. The torsion (S4) quantifies the change in the orientation of the local tangent plane along the filament. The angle δ gives that change in orientation one monomer distance, so that

$$\tau \approx \frac{\langle\delta\rangle}{d} \approx 0.11nm^{-1}. \tag{S6}$$

This value of the torsion, larger than the main curvature ρ, produces a very stretched helix. The projected radius $R \approx 2.2nm$ is similar to the diameter of each monomer, so that adding the monomer size along the helix, the FtsZ filament would fit into a cylinder of of about $3d \approx 13nm$, quite narrow compared with the typical lengths in the range of microns. A full round of the helix is completed over a distance $2\pi\lambda \approx 70nm$ measured along the cylinder (Z) axis, and about 182.5 monomers or $56nm$ measured along the helix.

The gaussian fluctuations of θ and δ, described by the values $\Delta\theta \approx 2.4^o$ and $\Delta\delta \approx 4^o$ given above, produce local changes in the local curvature and torsion, i.e. deformations of the helical structure. The parameters R and λ will fluctuate, both with time for any position along the filament and with the position for a given time. Given the stretched aspect of the helix, the most visible effect would be the fluctuation in the direction of the helical axis, i.e. in the global shape of the filament, that would fluctuate like a filament without any spontaneous curvature and showing a persistence length in the range of microns.

2 Model for elastic helical filaments anchored to a planar substrate

The shape of the FtsZ helix is described by the mean bending angle $\theta_o \equiv \langle\theta\rangle$ and the mean torsion angle $\delta_o \equiv \langle\delta\rangle$. The associated elastic constants $\kappa_\theta \equiv kT/(\Delta\theta)^2$ and $\kappa_\delta \equiv kT/(\Delta\delta)^2$ describe the flexibility of the free filaments. Here we consider how these properties may be reflected when the protein filament is adsorbed on a planar substrate.

We assume thermal average over the distance between monomers along the filaments, as well as on any internal structure of the monomers and on the solvent. Therefore we model the free energy of the filament as a function of the monomer orientations, to keep track of the on-plane shape and the internal torsion of the filament, which is the experimentally accesible information.

In the continuous limit, the structure of a perfect helix (S1) is given by the changes of the monomer orientations with respect to the distance s along the the filament,

$$\frac{d\mathbf{t}(s)}{ds} = \rho_o \mathbf{n}(s), \tag{S7}$$

and

$$\frac{d\mathbf{b}(s)}{ds} = -\tau_o \mathbf{t}(s), \tag{S8}$$

where the unit vector $\mathbf{t}$ gives the local longitudinal direction at any point along the filament, $\mathbf{n}$ gives the local orientation of the tangent plane, and $\mathbf{b} \equiv \mathbf{t} \times \mathbf{n}$ completes the local orthogonal basis. In our filament model we assume rigid monomers, so that the flexibility of the filaments is associated to the fluctuations in the interfaces of the monomers at the bond. The shape of the filaments would be given by the differences between the vectors $\mathbf{t}$, $\mathbf{b}$ and $\mathbf{n}$ that describe a monomers, and the vectors $\mathbf{t}'$, $\mathbf{b}'$ and $\mathbf{n}'$ that describe the next nomomer along the filament, separated by a distance σ. The local version of (S7) becomes

$$\frac{\mathbf{t}' - \mathbf{t}}{\sigma} = \rho \mathbf{n}, \tag{S9}$$

and

$$\frac{d\mathbf{b}(s)}{ds} = -\tau_o \mathbf{n}(s), \frac{\mathbf{b}' - \mathbf{b}}{\sigma} = -\tau \mathbf{t}, \tag{S10}$$

allowing fluctuation of the local curvature ρ and torsion τ, around their mean values ρ_o and τ_o.

The scheme in Fig.S2 shows the orientation of each monomer when the filament is anchored on a planar subtrate. The unit vectors $\mathbf{t}$ and $\mathbf{t}'$ have to be on that plane, i.e. they are perpendicular to the unit vector $\mathbf{v}$ normal to the substrate. The angle $\theta = cos^{-1}(\mathbf{t} \cdot \mathbf{t}')$ gives the local (on-plane) curvature of the filament, which in the free helix has the optimal value θ_o and fluctuations with amplitude $\delta\theta$ as described in the previous section.

The vectors $\mathbf{b}$ and $\mathbf{n}$, which give the torsional state of the filament, are decribed by the angle ψ on the plane formed by the fixed direction $\mathbf{v}$ and the local (on-plane) vector $\mathbf{u} = \mathbf{v} \times \mathbf{t}$,

$$\mathbf{b} = cos(\psi)\mathbf{u} + sin(\psi)\mathbf{v}, \tag{S11}$$

and

$$\mathbf{n} = -sin(\psi)\mathbf{u} + cos(\psi)\mathbf{v}. \tag{S12}$$

The torsion between two filaments is given by $\delta = \psi' - \psi$, which in the free filament would fluctuate around its mean value δ_o and with the typical deviation $\Delta\delta_o$.

The anchoring of the filament to a planar surface implies an elastic cost to keep the consecutive monomers with their $\mathbf{t}$ and $\mathbf{t}'$ axis on the plane. That elastic cost couples the torsion angles ψ and ψ' and we model that coupling through a simplified description of the interfaces of the monomers forming a bond. The (free) energy $U_{i,i+1}$, for the bond formed between the i and the $i+1$ monomer along the chain, depends on the orientation and relative positions of the two monomers. The restriction to have the filament absorbed on a substrate and with a preferential orientation of its secondary axis $\mathbf{b}_i$ represents an additional energy contribution an constraint. The equilibrium configuration corresponds to the minimum of the total energy with respect all the orientation variables, which is equivalent to balance the moments on each monomer, and the flexibility of the filaments is described in terms of the quadratic expansion of the energy around that minimal configuration. Notice that we do not have to consider the force balance on each monomer, since we assume thermal average over the (rapid) fluctuations of the instantaneous bond distances, as well as on any internal structure of the monomers and on the solvent. The flexibility arising from these fluctuations is embedded into the optimal configuration and effective elastic constants associated to the monomer orientations.

Despite that simplification, we still face a difficult problem to model the bond free energy $U_{i,i+1}$ as a function of the monomer orientations, with the limited information avaible from the atomistic MD simulations. Moreover, it is a hard mathematical problem to find the solution of the moment balance when the monomers are linked along a long filament and adsorbed on a substrate. In this section we present a simple model for the elasticity of the free filament, that allows us to get generic information for long filaments from the results of the atomistic Molecular Dynamics simulation of a pentamer. The shape of the filaments adsorbed on a planar substrate may be studied analitically only in the limit of very strong anchoring.

In the next section we analyze the detailed solution in the presence of a simplified model that allows to consider the arbitrary strength for that preferential orientation of the filaments.

To model the functional form of the bond (free) energy $U_{i,i+1}$, as a function of the monomers orientations, we assume (see Fig. S2) that each protein monomer has a + and a − interface, each one described by a vector $\mathbf{z}_i^{\pm}$ pointing outwards and perpendicular to the interface, and a vector $\mathbf{b}_i^{\pm}$ on the interfacial plane. The optimal state of the bond (with the minimum energy $U_{i,i+1} = -U_b$) is formed when the + interface of a monomer (i) is parallel to the − interface of the next monomer $(i+1)$ (i.e. $\mathbf{z}_{\mathbf{i+1}}^{-} = -\mathbf{z}_{\mathbf{i}}^{+}$), and when the the two vectors on the interfacial planes are aligned (i.e. $\mathbf{b}_{\mathbf{i+1}}^{-} = \mathbf{b}_{\mathbf{i}}^{+}$). Deviations from that optimal configuration would imply an increase of the energy above its optimal value, that we describe in terms of the bending and torsion elastic constants κ_θ and κ_δ, obtained from the MD simulation of the FtsZ pentamer, as

$$\begin{aligned} U_{i,i+1} &= -U_b + \kappa_\theta \left(1 + \mathbf{z}_i^{+} \cdot \mathbf{z}_{i+1}^{-}\right) + \kappa_\delta \left(1 - \mathbf{b}_i^{+} \cdot \mathbf{b}_{i+1}^{-}\right) \approx \\ &\approx -U_b + \frac{\kappa_\theta}{2} \left(\Delta\Theta_{i,i+1}\right)^2 + \frac{\kappa_\delta}{2} \left(\psi_{i+1} - \psi_i - \delta_o\right)^2, \end{aligned} \tag{S13}$$

where $\Delta\Theta_{i,i+1}$ is the orientational mismatch between the interfaces of the bonded monomer, $\mathbf{z}_i^{+} \cdot \mathbf{z}_{i+1}^{-} = -cos(\Delta\Theta_{i,i+1})$, and $\psi_{i+1} - \psi_i - \delta_o$ is the torsional mismatch between their secondary axis, $\mathbf{b}_i^{+} \cdot \mathbf{b}_{i+1}^{-} = cos(\psi_{i+1} - \psi_i - \delta_o)$.

The helix in the optimal free structure determines the relative orientation of the ± interfaces with respect to the molecular axis $\mathbf{t}$ and $\mathbf{b}$, so that the observed mean angles for bending and torsion θ_o and δ_o determined in the MD simulation of the FtsZ pentamer are reproduced with

$$\mathbf{b}^{+} = cos\left(\psi + \frac{\delta_o}{2}\right)\mathbf{u} + sin\left(\psi + \frac{\delta_o}{2}\right)\mathbf{v}, \tag{S14}$$

$$\mathbf{b}^{-} = cos\left(\psi - \frac{\delta_o}{2}\right)\mathbf{u} + sin\left(\psi - \frac{\delta_o}{2}\right)\mathbf{v}, \tag{S15}$$

$$\begin{aligned} \mathbf{z}^{+} &= cos\left(\frac{\theta_o}{2}\right)\mathbf{t} + sin\left(\frac{\theta_o}{2}\right)\mathbf{b}^{+} = \\ &= cos\left(\frac{\theta_o}{2}\right)\mathbf{t} + sin\left(\frac{\theta_o}{2}\right) cos\left(\psi + \frac{\delta_o}{2}\right)\mathbf{u} + sin\left(\frac{\theta_o}{2}\right) sin\left(\psi + \frac{\delta_o}{2}\right)\mathbf{v}, \end{aligned} \tag{S16}$$

and

$$\begin{aligned} \mathbf{z}^{-} &= -cos\left(\frac{\theta_o}{2}\right)\mathbf{t} + sin\left(\frac{\theta_o}{2}\right)\mathbf{b}^{-} = \\ &= -cos\left(\frac{\theta_o}{2}\right)\mathbf{t} + sin\left(\frac{\theta_o}{2}\right) cos\left(\psi - \frac{\delta_o}{2}\right)\mathbf{u} + sin\left(\frac{\theta_o}{2}\right) sin\left(\psi - \frac{\delta_o}{2}\right)\mathbf{v}. \end{aligned} \tag{S17}$$

The torsional energy at each bond is then given by

$$\kappa_\delta \left(1 - \mathbf{b}_i^{+} \cdot \mathbf{b}_{i+1}^{-}\right) = \kappa_\delta \left(1 - cos(\delta_o + \psi_i - \psi_{i+1}\right) \approx \frac{\kappa_\delta}{2} \left(\delta_o + \psi_i - \psi_{i+1}\right)^2 = \frac{\kappa_\delta}{2}(\delta_i - \delta_o)^2, \tag{S18}$$

so that under thermal equilibrium we recover the values of $\langle\delta_i\rangle = \delta_o$ and $\langle(\delta_i - \delta_o)^2\rangle = kT/\kappa_\delta$ observed in the free filament.

The bending energy, in terms of the on-plane angle θ between the directions of $\mathbf{t}_i$ and $\mathbf{t}_{i+1}$, takes the form

$$\kappa_\theta \left(1 + \mathbf{z}_i^+ \cdot \mathbf{z}_{i+1}^-\right) = \kappa_\theta \left(1 - A(\psi_i, \psi_{i+1})\ cos\left(\theta - \theta_M(\psi_i, \psi_{i+1})\right) + B(\psi_i, \psi_{i+1})\right), \tag{S19}$$

that reflects the effects of the substrate forcing the monomers to lie flat on its plane.

The optimal on plane angle is given by

$$\theta_M(\psi_i, \psi_i) = tan^{-1}\left[\frac{sin\theta_o\left(cos(\psi_i + \delta_o/2) + cos(\psi_{i+1} - \delta_o/2)\right)}{(1 - cos\theta_o) - (1 + cos\theta_o)cos(\psi_i + \delta_o/2)cos(\psi_{i+1} - \delta_o/2)}\right]. \tag{S20}$$

The other two coefficients in (S19) are given by

$$A(\psi_i, \psi_i) = \frac{1}{2}\left[(1 + cos\theta_o)^2 + \left(cos^2(\psi_i + \delta_o/2) + cos^2(\psi_{i+1} - \delta_o/2)\right) sin^2\theta_o + \right.$$
$$\left. + cos^2(\psi_i + \delta_o/2)cos^2(\psi_{i+1} - \delta_o/2)(1 - cos\theta_o)^2\right]^{1/2}, \tag{S21}$$

and

$$B(\psi_i, \psi_i) = \frac{1 - cos\theta_o}{2} sin(\psi_i + \delta_o/2)sin(\psi_{i+1} - \delta_o/2). \tag{S22}$$

When the angles $\psi_i + \delta_o/2$ and $\psi_{i+1} - \delta_o/2$ are very small, the natural tangential plane of the free filament is precisely on the substrate, so that the optimal on-plane angle is the same as in the free helix, $\theta_M(0,0) = \theta_o$. In that situation we find $A(0,0) = 1$ and $B(0,0) = 0$, so that the elastic on-plane bending constant is equal to that in the free helix,

$$\kappa_\theta \left(1 + \mathbf{z}_i^+ \cdot \mathbf{z}_{i+1}^-\right) = \kappa_\theta \left(1 - cos(\theta - \theta_o)\right) \approx \frac{\kappa_\theta}{2}(\theta - \theta_o)^2, \tag{S23}$$

and there is no bending energy, nor torque, done by the substrate to keep the bond on-plane.

In the opposite limit, when $\psi_i + \delta_o/2 = \psi_{i+1} - \delta_o/2 = \pm\pi/2$, the natural torsion plane of the free filament is perpendicular to the substrate plane, and we get $\theta_M(\pi/2, \pi/2) = 0$, i.e. there is no spontaneous curvature for the filaments on the plane. The on-plane elastic constant is slightly reduced, to a value $\kappa_\theta A(\pi/2, \pi/2) = \kappa_\theta(1 + cos\theta_o)/2$, but the most important effect is that the coefficient (S22) reaches its maximum value, as an effective anchoring free energy $\kappa_\theta B(\pi/2, \pi/2) = \kappa_\theta(1 - cos\theta_o)/2$, that penalizes those orientations of the secondary axis, $\mathbf{b}_i$ and $\mathbf{b}_{i+1}$ by the bending energy cost required to keep the main axis, $\mathbf{t}_i$ and $\mathbf{t}_{i+1}$, on the substrate plane. With the values $\beta\kappa_\theta \approx 583$ and $\theta_o \approx 7.6^o$ obtained from the MD of the FtsZ pentamer, this free energy is $\kappa_\theta B(\pi/2, \pi/2) \approx 3kcal/mol$, i.e. nearly $5kT$ at room temperature, which may be quite relevant to determine the preferential orientation (and hence the on-plane curvature) of filaments on planar substrates.

3 Independent-bonds simulations for anchored filaments

Obviously, on top of the effective anchoring energy $\kappa_\theta B(\psi_i, \psi_i)$ induced by the bending, the direct interaction with the FtsZ monomers with the surface of mica, or their attachment to lipid membranes would represent a free energy contribution $u_a(\psi)$ per monomer. We have

explored the thermal equilibrium distributions for filaments with the bending and torsional energy given by (S13), and under a simple anchoring potential model,

$$u_a(\psi) = min\left(0, -U_a + \frac{\kappa_\psi}{2}(\psi - \psi_o)^2\right), \tag{S24}$$

with the minimum free energy $-U_a$ when the monomers have the orientation ψ_o, and with a stiffness controlled by κ_ψ. This term, added for all the monomers in a filament $\sum_i u_a(\psi_i)$, describes the specific anchoring of the protein monomers that depends on the nature of the substrate, and on how the protein is linked to it. As a free energy that depend on the monomers orientations it has to be added to the generic contribution, proportional to the bending rigidity of the free filament (S19), that comes from the geometrical constrain to force the free filament helix on the substrate plane.

We have done simulations to get the thermal equilibrium structure of filaments under different choices of the specific anchoring potential, added to the generic contribution that may be extracted from the helical structure and elasticity of the free filament. The simulations were done for *ideal filaments*, i.e. neglecting any interaction beyond the independent structure of each bond. The monomers were added, one by one, to the end of the chain with the orientations ψ_i, ψ_{i+1},..., chosen to reproduce the equilibrium probability distribution in their torsional state. The on-plane shape of the filament was then obtained with independent gaussian distributions for the on-plane bending angle θ_i, with mean value given by $\theta_M(\psi_i, \psi_{i+1})$ in (S20) and mean square fluctuations $\langle(\theta_i - \theta_M(\psi_i, \psi_{i+1}))^2\rangle = kT/(\kappa_\theta A(\psi_i, \psi_{i+1}))$, with the effective on-plane bending (S21). We have constructed many long filaments, up to $N = 50000$ monomers, although they should be considered representative only for those properties that involve the statistical configurations of independent bonds. The sketches shown in Fig. S3 shows typical shapes for shorter filament shapes, for which the independent bond description is realistic. We have used $\beta U_a = 45$, and different values of the preferential angle ψ_o and stiffness κ_ψ in the anchoring potential (S25). From the observed shapes, it is clear that a broad range of anchoring parameters would lead to the formation of rings (if the model filament were allowed to form a closing bond), or rolls with multiple rounds (if the effects of the excluded area and the lateral attraction between the filaments were included). The frequent observation of these shapes in FtsZ filaments on planar substrates may therefore be explained as a result of the planar constraint imposed on the helical free filaments, with the generic bond structure and elasticity represented by (S13). The effect of specific anchoring may be found in the variation of the mean on-plane angle $\langle\theta_i\rangle = \langle\theta_M(\psi_i, \psi_{i+1})\rangle$, or equivalently in the optimal ring radius $\langle R\rangle = \sigma/\langle\theta\rangle$ for monomers of size σ. For very stiff anchoring, i.e. large κ_ψ in (S25), all the monomers would have similar orientation $\psi_i \approx \psi_o$ and the mean curvature of the filaments would be determined by (S20). When the optimal anchoring on the substrate keeps the orientations of the tangential plane in the free filament (i.e.$\psi_o \approx 0$) the filaments would have their maximum curvature $\langle\theta\rangle \approx \theta_o$. Increasing ψ_o reduces the mean curvature, since the anchoring on the planar substrate forces the filament partially out of its spontaneous curvature as a free helix. For large enough values of ψ_o, the combined effect of the anchoring on the substrate and the spontaneous torsion along the filament, lead to reach $\langle\theta\rangle = 0$, i.e. flexible filaments without spontaneous on plane curvature. Further increase of ψ_o produce filaments with the opposite curvature.

Fig. S4(a) presents the mean on-plane angle $\langle\theta\rangle$, as a function of the anchoring stiffness, for several preferential anchoring orientations. For large values of κ_ψ the dependence with

ψ_o follows the qualitative trend described above, a value of $\psi_o = 0$ gives the maximum curvature $\langle\theta\rangle \leq \theta_o = 7.6^o$ when $\beta\kappa_\psi \geq 500$, while larger values of $\psi_o = 0$ gradually reduce the curvature. In the opposite limit, for very loose anchoring with $\beta\kappa_\psi \leq 50$, the mean curvature of the filaments is always very small, and it changes very little with the value of ψ_o. That effect is produced by the spontaneous torsion of the filament, that tends to keep the angle ψ_i changing along the filament, so that regions with $\psi_i \approx 0$ and others with $\psi_i \approx 180^o$ cancel out the mean curvature of the filament. The main change of $\langle\theta\rangle$ with respect to the surface stiffness is observed over the range $350 \leq \beta\kappa_\psi \leq 800$. Thus, the spontaneous angle observed in FtsZ filaments on mica [1, 2], $\langle\theta\rangle \approx 2.5^o$ would be compatible with the elasticity of the helix observed in the MD simulation of the FtsZ pentamer, and with anchoring potentials (S25) below $\beta\kappa_\psi \approx 400$ (region a in Fig. S4). The observation of larger curvatures (i.e. smaller radius) would be predicted for stiffer anchorages and low ψ_o (regions b and c in Fig. S4

The observation of very straight FtsZ filaments requires not only the cancellation of the mean angle $\langle\theta\rangle \approx 0$, it is also needed a large on-plane bending modulus $\beta\kappa = (\langle\theta^2\rangle - \langle\theta\rangle^2)$, so that all the bond angles fluctuate very narrowly around their mean value $\theta_i \approx \langle\theta\rangle$. Fig. S4(b) presents the results for $\beta\kappa$ from our simulations, that (as may be predicted from (S21)) depends very little on ψ_o, so that the averaged results are presented in a single curve as a function of the anchoring stiffness. The rigidity of the free helix is shown in the large value $\beta\kappa \geq 600$ observed for stiff anchoring ($\beta\kappa_\psi \geq 800$), when the variations of the on-plane angle are directly associated to the deformations of the free helix. However, for looser anchoring potentials the on plane angle fluctuates much more from the fluctuations of ψ_i (relative orientation with respect to the substrate) than from the deformations of the filament. The effect is that the effective on-plane rigidity is stabilized at $\beta\kappa \approx 100$ for $\beta\kappa_\psi \leq 400$. The fluctuations of short FtsZ filaments on mica where used to estimate $\beta\kappa \approx 90 - 100$ [2] and that value would be reached for $\beta\kappa_\psi \leq 400$, in good agreement with the range of anchoring stiffness compatible with the observed mean curvature.

4 Polymorphism in twisted filaments

The experimental observation of FtsZ filaments shows the dependence of their mean curvature on the type of attachment to the surface [3], and we have seen above how that dependence may be explained in terms of the torsional structure of the filaments. The AFM images do not have resolution to show the orientation of the protein monomers but, within a simple model for the coupling between the filament torsion and its on-plane shape, we may correlate the observed spontaneous curvature and the flexibility of the filaments to the thermal distribution of the torsion angles. Here we explore how the same model may account for recent experimental observation of FtsZ filaments on mica [4] that show the coexistence of short filaments with straight and curved shapes, when their growth and mobility is stopped suddenly. That is something difficult to reconcile with the fluctuations around a well defined and fixed filament curvature, and the answer may come from the existence of different torsional metastable states, that could be reflected in different on-plane shape of the filaments.

The filament shapes described in the previous section correspond to the thermal equilibrium configurations of the bonds, treated as being fully independent of each other. That

ideal-polymer treatment is accurate to get the mean curvature and the bending modulus from the shape of short filaments, but it cannot be used to discern between globally different configurations that may be observed if the filament is trapped in a metastable state, from which it can only scape through a global change involving major changes in the torsional structure of the whole filament, high free energy barriers and slow dynamics. To explore qualitatively this effect, we present here a simple modelization in which we keep the quadratic torsional energy (S18). The generic anchoring anisotropy induced by the bending of the free helix into a flat shape (S19) and the substrate specific anchoring potentials (S25) are described together as a simple effective free energy

$$U_a = -\kappa_a \sum_{i=1}^{N} cos(\psi_i - \psi_o), \tag{S25}$$

with minimum for $\psi_i = \psi_o$ and a quadratic

The total torsional free energy of a filament with N monomers is taken as

$$U(\psi_1, \psi_2, ..., \psi_N) = \frac{\kappa_\delta}{2} \sum_{i=1}^{N-1} (\psi_{i+1} - \psi_i - \delta_o)^2 - \frac{\kappa_a}{2} \sum_{i=1}^{N} cos(\psi_i - \psi_o), \tag{S26}$$

and the local minima with respect to the monomers orientations is given by

$$\frac{\partial U(\psi_1, \psi_2, ..., \psi_N)}{\partial \psi_i} = -\kappa_\delta(\psi_{i+1} - 2\psi_i + \psi_{i-1}) + \kappa_a sin(\psi_i - \psi_o) = 0, \tag{S27}$$

for any inner monomer $2 \leq i \leq N-1$ along the chain, while for those at the ends we have

$$\frac{\partial U(\psi_1, \psi_2, ..., \psi_N)}{\partial \psi_1} = -\kappa_\delta(\psi_2 - \psi_1 - \delta_o) + \kappa_a sin(\psi_1 - \psi_o) = 0 \tag{S28}$$

and

$$\frac{\partial U(\psi_1, \psi_2, ..., \psi_N)}{\partial \psi_N} = \kappa_\delta(\psi_N - \psi_{N-1} - \delta_o) + \kappa_a sin(\psi_N - \psi_o) = 0. \tag{S29}$$

In the limit of smooth variations in the orientation of the monomers along the chain, we may use the monomer size d to express ψ_i as a continuous function $\psi(t)$, in terms of the filament length, $t = di$ for the monomer i, and take the continuous limit of (S27) to get

$$\frac{\partial^2 \psi(t)}{\partial t^2} = \frac{\kappa_a}{\kappa_\delta d^2} sin(\psi(t) - \psi_o), \tag{S30}$$

which has an intuitive mechanical analogue in the equation of a pendulum, where t plays the role of time, $\kappa_a/(\kappa_\delta d^2)$ is equivalent to the ration between gravity acceleration and the pendulum length, and the angle $\psi = \psi_o$ corresponds to the unstable top position of the pendulum. The minimum with respect to the orientation of the monomers at the ends of the filament (S29) correspond in the continuous limit to set fixed angular velocities

$$\left.\frac{\partial \psi(t)}{\partial t}\right|_{t=0,Nd} = \frac{\delta_o}{d} \equiv \omega_o \tag{S31}$$

at the *initial* $t = 0$ and at the *final* $t = Nd$ times.

This mechanical analogue gives the clue to understand the possible existence of multiple local minima, i.e. multiple solutions of (S27-S29). In absence of anchoring effects ($\kappa_a = 0$ in (S26)-S29), the filament has minimum free energy when all the bonds have the optimal torsion $\psi_{i+1} - \psi_i = \delta_o$. The mechanical analogue is the free rotation, with constant angular velocity $d\psi(t)/dt = \omega_o$, of a rotor in absence of any gravity effect. A filament made of N monomers would have $N\omega_o/(2\pi)$ full torsion rounds, equivalent to the full rounds of the free rotor in a 'time' $t = Nd$. The gravity makes the rotor to go slower (i.e. the twist rate of the filament is less than optimal) in the upper side of the cycle (i.e. in the well-anchored portions of the filament), and the rotor goes faster (i.e. the filament is over-twisted) in the *lower* side of the cycle (i.e. when the orientation of the monomers is opposite to their optimal anchoring). If the filament is long enough, there are other local minima of (S26) that correspond to unwound any number of torsional rounds, or in the pendulum analogue to have a lower rotor, that is started with the same angular velocity ω_o but from a lower position, so that it needs a longer time to make each round, and it completes a lesser number of rounds in the time $t = Nd$. The final state of that unwinding series of metastable configurations corresponds to a well-anchored filament, fully unwound, in which nearly all the monomers at very close to their optimal anchoring orientation, and only those near the ends show a small relaxation to their natural torsion.

The model may explored quantitatively, by means of the first integral of (S30), the constant total energy of the pendulum,

$$E \equiv \frac{\kappa_\delta d^2}{2}\left(\frac{\partial\psi(t)}{\partial t}\right)^2 + \kappa_a cos\left(\psi(t) - \psi_o\right), \tag{S32}$$

that is fully determined by the initial the known angular velocity $\omega_o = \delta_o/d$ and the unknown initial angle $\psi(0) \equiv \psi_1$ (i.e. the orientation of the first monomer in the filament). Then we may integrate

$$\frac{\partial\psi(t)}{\partial t} = \left[\omega_o^2 + \frac{\kappa_a}{\kappa_\delta d^2}\left(cos\left(\psi(0) - \psi_o\right) - cos\left(\psi(t) - \psi_o\right)\right)\right]^{1/2} \tag{S33}$$

to get the analytical implicit solution for the orientation of each monomer $\psi_j = \psi(t_j)$ as an elliptic function,

$$(j-1)d \equiv t_j = \int_{\psi_1}^{\psi_j} d\psi \left[\omega_o^2 + \frac{\kappa_a}{\kappa_\delta d^2}\left(cos\left(\psi_1 - \psi_o\right) - cos\left(\psi - \psi_o\right)\right)\right]^{-1/2}. \tag{S34}$$

The value of ψ_1 has to be found to get $\partial\psi(t)/\partial t = \omega_o$, at the other end of the filament $t = (N-1)d$, or equivalently $cos\left(\psi_N - \psi_o\right) = cos\left(\psi_1 - \psi_o\right)$. In practice it is simpler to use ψ_1 as a parameter, to get from (S34) the time t compatible with $\psi(t) - \psi - o = \psi_o - \psi(0)$, and consider the multiple solutions that may be obtained by adding to t any number of periods

$$T(\psi_1)) = \int_0^{2\pi} d\psi \left[\omega_o^2 + \frac{\kappa_a}{\kappa_\delta d^2}\left(cos\left(\psi_1 - \psi_o\right) - cos\left(\psi - \psi_o\right)\right)\right]^{-1/2}. \tag{S35}$$

For any filament which is long enough, we may find several several values of ψ_1 represent different local minima of (S26). In Fig. S5 we present the energy per monomer at the

different local minima of (S26) that are found for filaments up to $N = 200$ monomers. The deep minimum on the left corresponds to *well anchored* filament, in which the orientation of all the monomers is kept close to the optimal anchoring $\psi_j \approx \phi_o$, unwinding the natural torsion $\psi_{j+1} - \psi_j = \delta_o$ of the filament, so that $\phi_N - \phi_1 < 2\pi$. For short filaments, $N \leq 30$ that is the only local minimum, and therefore the thermal fluctuations of the filament would produce torsional structures around that configuration. However, for larger filaments we find another local minimum of (S26) in which the orientation of the monomers cover a full round, i.e. $2\pi < \psi_N - \phi_1 < 4\pi$. That configuration becomes the absolute minimum for a range of filament length, but still the fully anchored configuration persist as a local minimum, and a new local minimum with $4\pi < \psi_N - \phi_1 < 6\pi$ appears for $N \geq 60$ to become the absolute minimum for longer filaments, and so on. The relative positions of each torsional configuration depend on the values of $\kappa_a/(\kappa_\delta d^2)$ and $\omega_o = \delta_o/d$, but in any case the existence of different local minima is a generic property of the balance between the spontaneous torsion of the free filament and the preferential orientation for the monomers on the planar substrate.

EXPERIMENTAL SECTION

4.1 Site-directed mutagenesis and overexpression of the S255C-EcFtsZ

For details of the procedure followed see [8]. In brief, the pET28a derivative plasmid pMFV56 16 eith the EcFtsZ gene under the control of a T7 promoter was used as the PCR template. Primers were designed to introduce the cysteine mutation accompanied by silent mutations that encode the marker restriction site for NarI. The primer used to generate S255C-EcFtsZ was primS255C (GCCACACAGGTCGATATCTTCCAGCAGAG) and primNarIb (GCCCGCGGCGTGCTGGTTAACATCACGGC).The primer was phosphorylated using E. coli E.D. pFDX Polynucleotide kinase (Roche Molecular Biochemicals). PCR products were amplified using the Excite High Fidelity PCR system (Roche) and purified with the Concert Rapid PCR Purification System (Life Technologies, Inc.) and polished with Pwo DNA polymerase (Roche) to remove any additional nucleotides added to the 3'end of the PCR product. The polished PCR product was purified and ligated by T4 DNA Ligase (Roche) transformed into E. coli DH5 cells and grown on L B plates containing 50 g/ml kanamycin. Plasmid DNA was purified from individual transformants and the mutant plasmid pAKV4 (pET28a-S255C-EcFtsZ) was identified by digestion with NarI. The presence of the mutation in the EcFtsZ gene was then confirmed by sequencing with the primers ak1 (GTTTGTCGTTCGGGATAGTG), ak2 (CTGGAAGATATCGACCTCTCTGGC), and mf3 (GCACCAGTCGTCGCTGAAGTGGCA).

Overexpression of S255C-EcFtsZ was initially tested by transforming pAVK4 into the E.coli strains BL21(DE3) and C41(DE3) 17. S255C-EcFtsZ mutant genes were cloned into the lambda-promoter expression vector pND706 18. The gene was PCR amplified using the primers EcFtsZnde (GGAGAGAACATATGTTTGAACCAATGGAAC) and EcFtsZXhoI (TCCAGTCTCGAGTTAATCAGCTTGCTTACGC) to incorporate an NdeI site before the start codon and an XhoI site after the stop codon. Digestion of the resulting PCR products with NdeI and XhoI enabled cloning into pND706 to create pAVK6 (pND706-S255C-EcFtsZ). These constructions were checked by DNA sequencing as before. E. coli C43(DE3) cells 17 transformed with pAVK6 were grown at 30C in LB broth supplemented with 50 μg/ml ampicillin to an A595 of 0.5. Synthesis was induced by rapid shift of each culture to 42C and maintained for 3 hours.

References

[1] Hörger,I.; E.Velasco; J.Mingorance; G.Rivas;P.Tarazona and M.Vélez(2008) Langevin computer simulations of bacterial protein filaments and the force-generating mechanism during cell division. *Phys. Rev. E* 77:011902

[2] Hörger,I; E.Velasco; G.Rivas; M.Vélez and P.Tarazona (2008)FtsZ Bacterial Cytoskeletal Polymers on Curved Surfaces: The Importance of Lateral Interactions *Biophysical Journal*94:L81 - L83

[3] Mateos-Gil,P.;I. Márquez; P.López-Navajas; M.Jiménez; M.Vicente; J. Mingorance; G.Rivas and M. Vélez(2012)FtsZ polymers bound to lipid bilayers through ZipA form

dynamic two dimensional networks *Biochimica et Biophysica Acta (BBA) - Biomembranes* 1818: 806 - 813

[4] Hamon, L.; D.Panda; P.Savarin; V.Joshi; J.Bernhard, E.Mucher; A.Mechulam; P.A.Curmi and D.Pastré(2009)Mica Surface Promotes the Assembly of Cytoskeletal Proteins *Langmuir*25:3331-3335

[5] Allard, J.F. and E.N.Cytrynbaum(2008) Force generation by a dynamic Z-ring in Escherichia coli cell division. *Proc Natl Acad Sci USA* 106:145-150

[6] Lan, G. ; B.R.Daniels; T.M.Dobrowsky; D.Wirtz and S.X.Sun(2009) Condensation of FtsZ filaments can drive bacterial cell division *Proc Natl Acad Sci USA* 106:121-126

[7] Ghosh, B and A.Sain(2008) Origin of Contractile Force during Cell Division of Bacteria *Phys. Rev. Lett.* 101:178101

[8] Encinar,M.,A.Kralicek,A.Martos,M.Krupka,A.Alonso,S.Cid,A.I.Rico,M.Jiménez and M.Vélez (2013) Polymorphism of FtsZ filaments on lipid surfaces: role of monomer orientation *Langmuir*10.1021/la401673z

[9] Hess, B. (2002). Convergence of sampling in protein simulations. *Phys Rev E* 65:031910-031910.

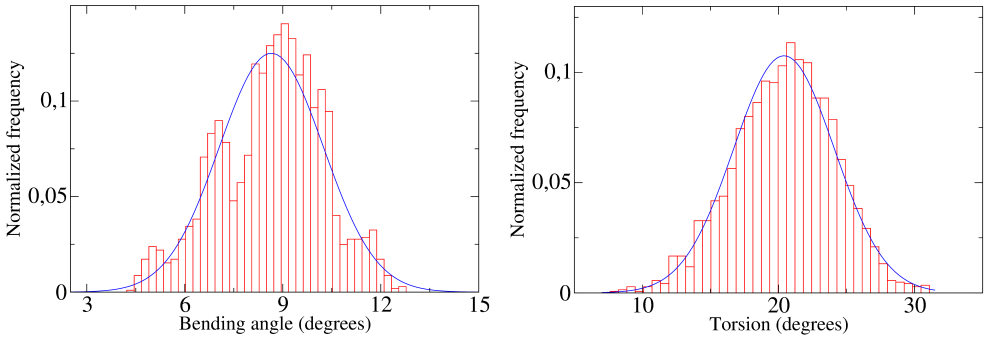

Figure S1: Histograms and gaussian fits for the distribution of bending, $(\pi - \alpha)/2$, and torsion (δ) angles obtained from the sampling over 5.24 nanoseconds, after an equilibration time of 4 nanoseconds, along the MD simulation of the FtsZ pentamer.

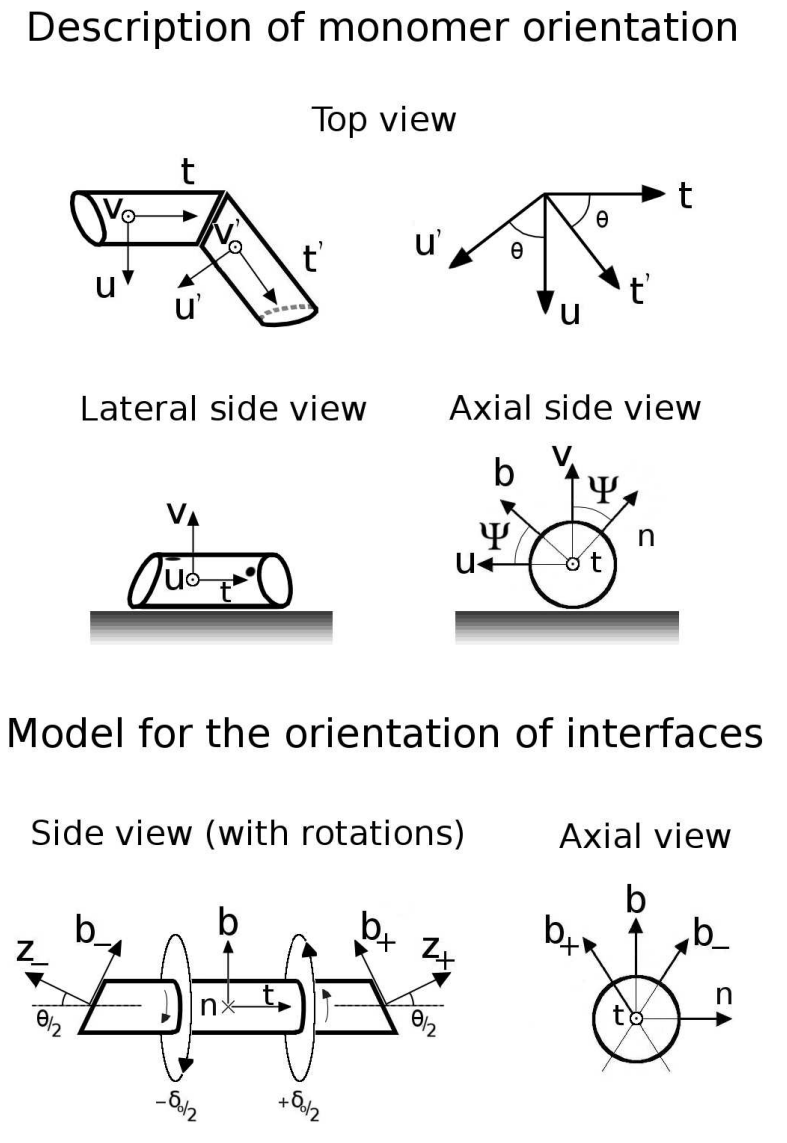

Figure S2: Scheme of the unit vectors used to describe the longitudinal axis of each monomer, **t** that defines the local tangent direction of the filament. The secondary axis **b** is on the plane perpendicular to **t**, and describe in term of the basis formed by the (fixed) direction **u** (normal to the substrate plane), and the (local) direction **v** on the substrate plane and perpendicular to **t**. The angle ψ, between **b** and **u**, gives the torsional structure of the filament as the difference $\delta = \psi' - \psi$ between neighbour monomers, and the angle θ on the substrate plane gives the change in the longitudinal directions of those monomers. The lower panels give the lateral and axial view of the model described in the text to represent the geometrical coupling between the torsional and the bending structures.

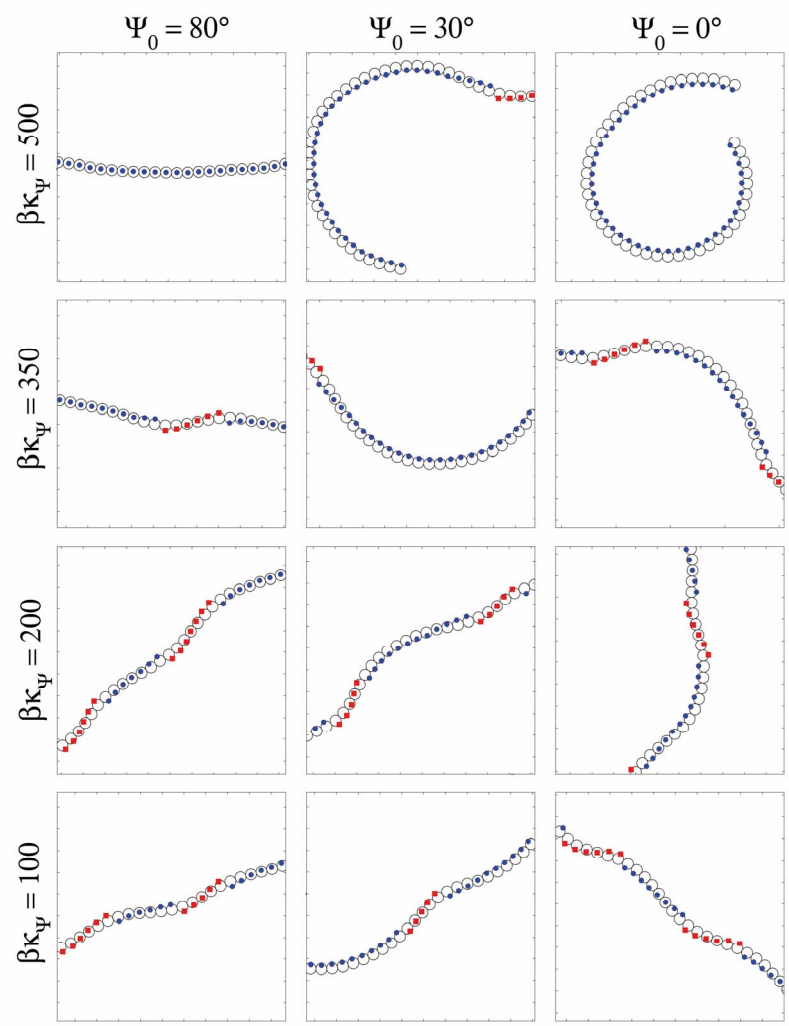

Figure S3: Typical shapes of FtsZ filaments on a planar substrate, obtained from the independent bond distribution model, with the helix parameter and elastic constants obtained from the fluctuations of the free pentamer, under different parameters for the anchoring of the protein monomers on the substrate.

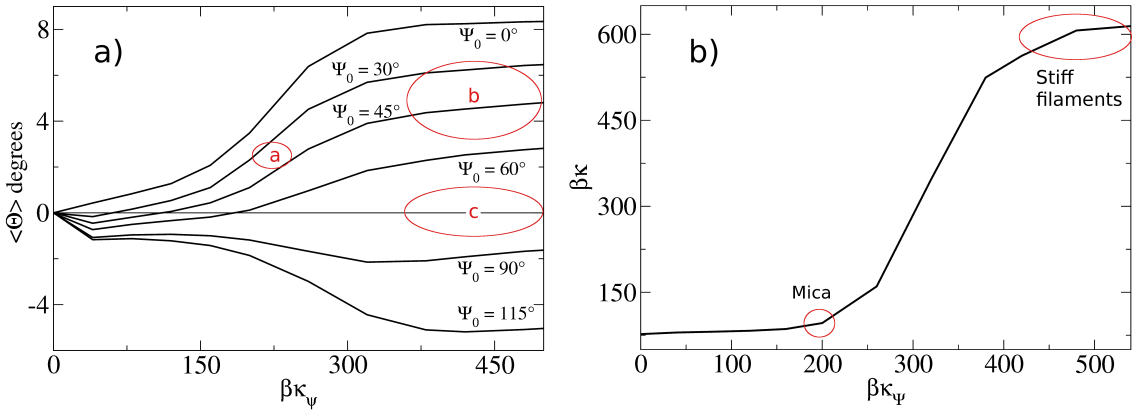

Figure S4: The on-plane mean angle (left) and bending rigidity (right) from our model of FtsZ filament under different parameters of the anchoring potential.Region a corresponds to the curvature observed on mica [1, 2]. See text for explanation of regions b and c

.

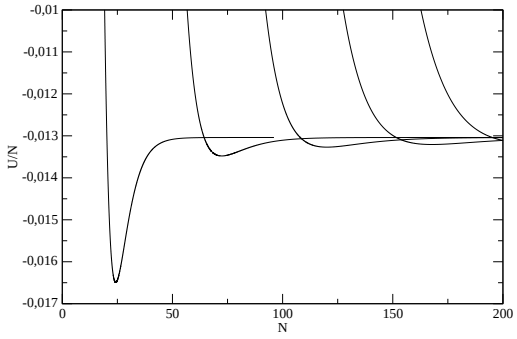

Figure S5: Free energy per monomer as a function of the number of monomers in the filament. Lines from left to right represent increasing number of full filament turns

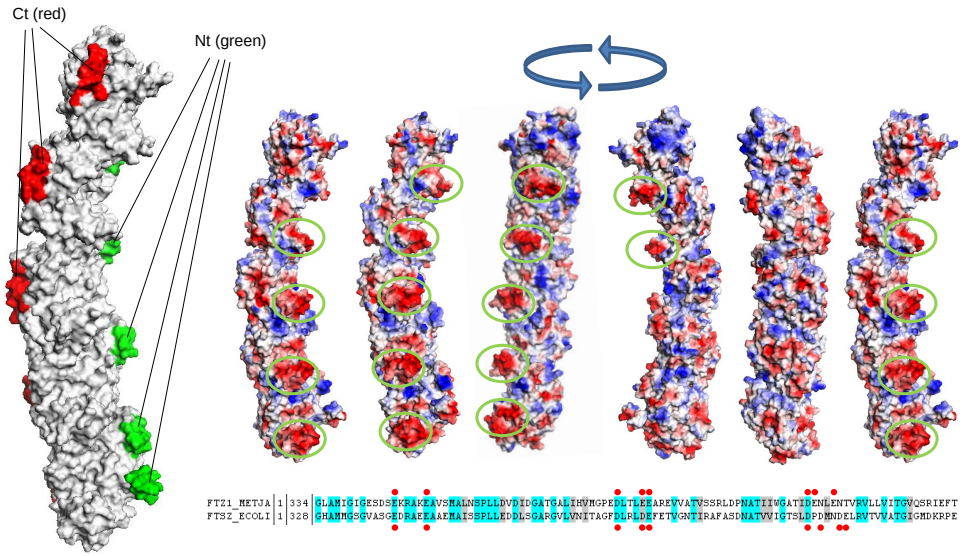

Figure S6: The diagram depicts in red the negatively charged aminoacids in FtsZ from Methanococcus Jannaschii and indicates that they are also conserved en E.coli FtsZ.

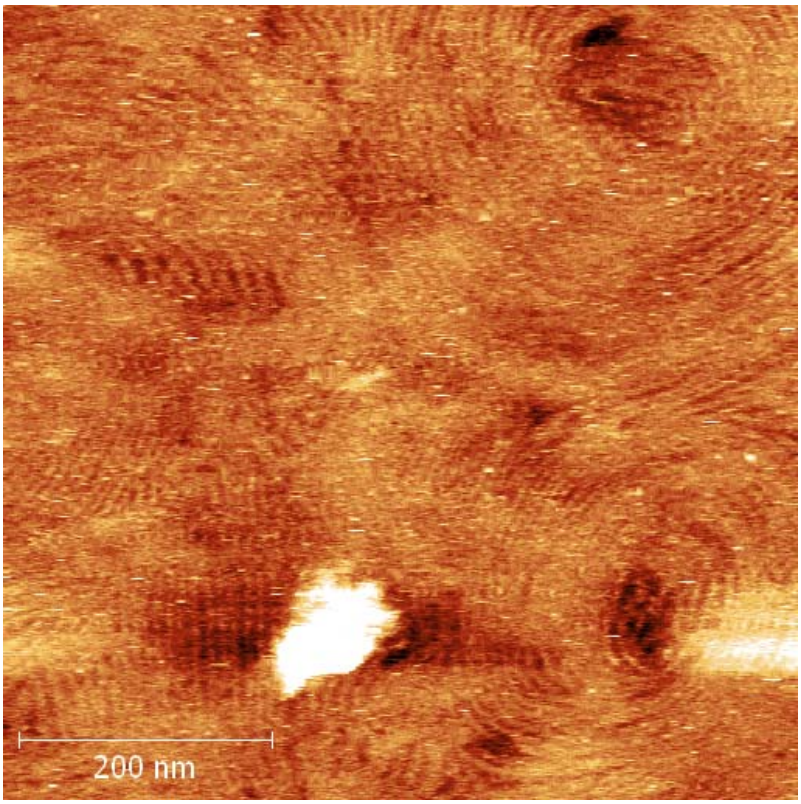

Figure S7: FtsZ cysteine mutant S255 , when anchored to the lipid bilayer through cysteine 255 to maleimide lipids forms curved filaments when a negatively charged lipid is included in the membrane. Lipid membrane composition is E.Coli polar lipids 90% / DSPE-Mal 10%. E.coli polar lipids contain about 30 % negatively charged lipids

.

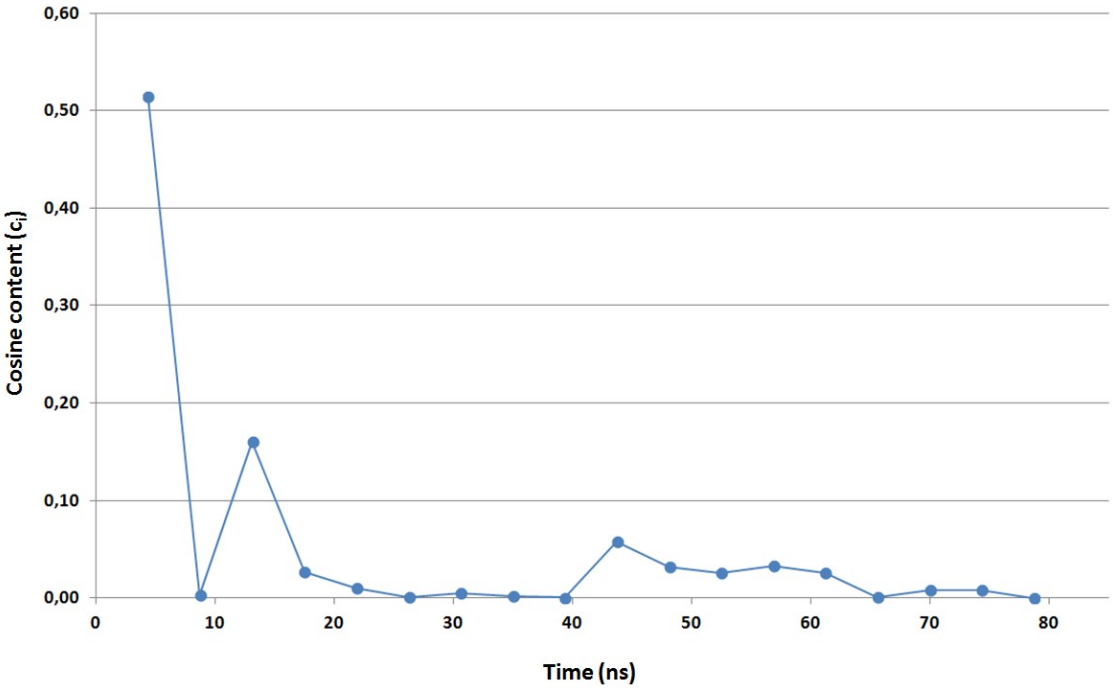

Figure S8: Evolution of the cosine content calculated for the first principal component in an 80 ns trajectory. Cosine content (ci) was calculated according to [9]. Covariance matrix was calculated using the c-alpha atoms of the whole structure. A fast decrease of the cosine content is observed in the first 20 ns, providing an information about the possible convergence the structure, and therefore, independent of the random diffusion.